Cryst. Res. Technol. **42**, No. 4, 325 – 332 (2007) / **DOI** 10.1002/crat.200610823

Mathematical modeling of the multi-run process of crystal pulling from the melt by EFG (Stepanov) technique in dependence on the angle of inclination of the working edges of the dies

A. V. Zhdanov[1], S. N. Rossolenko*[1], and V. A. Borodin[2]

[1] Institute of Solid State Physics of RAS, Chernogolovka, Moscow district, 142432, Russia
[2] Experimental Factory of Scientific Engineering of RAS, Chernogolovka, Moscow district, 142432, Russia

Received 13 September 2006, revised 11 December 2006, accepted 18 December 2006
Published online 10 March 2007

Key words multi-run process, modeling, EFG, sapphire.
PACS 47.27.Te, 44.40.+a, 81.10.Aj

A mathematical model for the determination of melt hydrodynamics, impurity concentrations and thermal stresses in the multi-run process of the growth of sapphire ribbons by EFG (Stepanov) technique with inclinated working surfaces of the dies is considered. The mathematical model deals with thermal conductivity equation, Navier-Stokes equation, diffusion equation, capillary Laplace equation. This problem has been solved by the finite-element method.

1 Introduction

The use of EFG (Stepanov) technique increases significantly productivity of the crystal growth process. At the same time multi-run growth technique requires a fine adjustment of the thermal field inside a heat zone and an optimum design of the dies assembly. This paper considers simultaneous growth of several sapphire ribbons with dies using various angles of inclination of its working edges on the basis of mathematical modeling. The paper continues the earlier published ref. [1] and deals basically with determination of hydrodynamics of the melt, impurity concentrations and thermal stresses in the each ribbon of the package in dependence on the angle of inclination of the dies working edges. In many cases position and shape of the crystallization front is very important. The angle of inclination can make significant influence on the crystallization front. Therefore, this paper considers also behavior of the interface boundary of the growing ribbons. The radiative heat exchange between lateral surfaces of the ribbons is supposed.

The goal of the finite element analysis is to determine the parameters of the pulling process minimizing the following: 1) the difference in temperature distribution of the packed ribbons to ensure growth control by heating power changes, 2) the magnitude of impurity concentration at local regions of the interface boundary near the lateral surface of the ribbons, 3) the magnitude of thermal stresses in each ribbon of the package to prevent block formation.

Solution technique of the whole problem consists of the sequence of iterative procedures to ensure condition of the constancy of the growth angle and agreement of the temperatures of the lateral surfaces of the ribbons with their densities of the radiative flows.

2 Model formulation

We shall take into account the fact that the heat transfer problem needs to be formulated individually for all the inner ribbons of the package and the two outer ribbons. This distinction originates from the difference of

* Corresponding author: e-mail: ross@issp.ac.ru

thermal exchange between the lateral surfaces of adjacent inner ribbons and these of the two outer ribbons with the neighboring medium.

A diagram of the crystallization process and the choice of the coordinate system are shown in figure 1. Indices 1 and 2 denote the quantities referring to the melt and crystal, respectively.

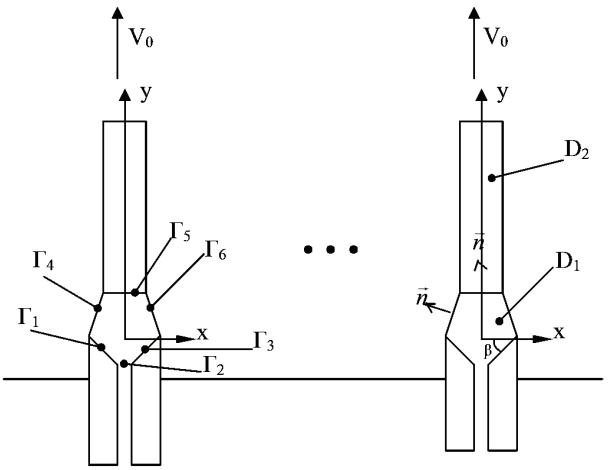

Fig. 1 General scheme of the multi-run pulling process by EFG (Stepanov) technique. Points signifies inner crystals.

The distribution of temperature in the regions D_1 and D_2 involving the melt in the meniscus and the crystal is described by the thermal conduction equation:

$$\Delta T_i - \zeta_i(V_i, \nabla T_i) = 0\,,\ (x,y) \in D_i\,,\ \zeta_i = \frac{\rho_i c_i}{k_i}\,,\ \text{i=1, 2,} \tag{1}$$

here $V_1 = (u_1, v_1)$ is the field of the melt rates in the meniscus and $V_2 = (0, V_0)$ is the rate of pulling.

At the interface boundary $H(x)$ the Stefan condition should be satisfied:

$$k_2(\vec{n}, \nabla T_2) - k_1(\vec{n}, \nabla T_1) = \rho_2 V_0 \Delta H_f (1 + H_x'^2)^{1/2}\,, \tag{2}$$

$$T_1[x, H(x)] = T_2[x, H(x)] = T_m\,,\ -h_1 \le x \le h_2\,,\ y = H(x)\,. \tag{3}$$

For the two lateral surfaces of the outer ribbons heat transfer from the melt and the crystal to the ambient at temperature $T_c(y)$, which depends only on the height, is accomplished by convection and radiation:

$$-k_i \frac{\partial T_i}{\partial \vec{n}} = \eta_i\ (T_i - T_c) + \sigma \varepsilon_i (T_i^4 - T_c^4)\,, \tag{4}$$

The equations describing radiative heat exchange between the lateral surfaces of adjacent inner ribbons will be derived below.

At the top face and the top of the crystal the following temperatures are preset:

$$T_1\big|_{\Gamma_1} = T_f + \frac{x}{\cos\beta}(T_c - T_f)\,,\ T_2(x, l) = T_2^0(x)\,,\ -h_1 \le x \le h_2\,. \tag{5}$$

The temperature T_1 decreases linearly from T_f to T_c over Γ_1, is constant over Γ_2 and equal T_c and increases linearly from T_c to T_f.

The right-hand profile curve of meniscus $f(y)$ satisfies the Laplace equation and the boundary conditions:

$$\rho_1 \mathrm{g(y + H_{ef})} = \sigma_{\mathrm{liq,g}} \frac{\mathrm{d}}{\mathrm{dy}}\left[\frac{\mathrm{df/dy}}{(1 + (\mathrm{df/dy})^2)^{1/2}}\right], \tag{6}$$

$$f(0) = a\,,\ -\left.\frac{df}{dy}\right|_{y=H(h_2)} = tg\varepsilon_0\,. \tag{7}$$

A similar equation describes the other curve. Both equations have the same value of external pressure H_{ef}.

The rate field in the melt $V_1 = (u_1, v_1)$ satisfies Stokes equations:

$$\mu\Delta V_1 + \rho_1(V_1,\nabla)V_1 = \nabla P + F\ ,\ F = (0, -\rho_1 g)\,, \tag{8}$$

$$divV_1 = 0\,. \tag{9}$$

Equation (9) allows to introduce a stream function ψ with usual technique. The behavior of the melt flow will be described further in her terms.

Boundary of the area D_1 consists of 6 sections (Γ_i, i = 1,...,6) in which boundary conditions are given according to the melt flow.

At the interface boundary $y = H(x)$ (Γ_2) we have :

$$V_{1n} = V_0\left[1 + (H_x^{'})^2\right]^{1/2}\ ,\ V_{1\tau} = 0\,. \tag{10}$$

Over the boundaries Γ_4 and Γ_6 that appropriate to the melt free surface, the normal component of the rate tends to zero, and besides the tangent strain tends to zero :

$$V_{1n} = 0\,,\ \left[(\vec{\tau}, D^{'}V_1), \vec{n}\right] = 0\ ,\ x = f(y)\,. \tag{11}$$

Boundaries Γ_1, Γ_3, Γ_2 that correspond to the die top face and to the outlet of a capillary gap satisfy the following:

$$u_1 = 0,\ \ v_1 = 0\,,\ (x,y) \in \Gamma_1 \cup \Gamma_3\,,\ u_1 = 0\,,\ v_1 = AV_0\left[1 - \left(\frac{x}{d_0}\right)^2\right],\ (x,y) \in \Gamma_2 \tag{12}$$

Constant A involving in the expression (12) may be determined from the condition of the equality of the melt streams through the capillary channel (boundary Γ_2) and crystallization front (boundary Γ_5). This constant is equal :

$$A = \frac{3}{4d_0}\int_{-b}^{b}(1 + H^{'2}(x))dx\,. \tag{13}$$

We consider the lateral surfaces of all ribbons to be diffuse-gray. This means that a part of an incident radiative flux $q_{i,k}(r_k)$ is mirrored evenly in all directions by lateral surface of a ribbon. The resultant radiative flux $q_k(r_k)$ for the surface area with a position vector r_k should be written as follows:

$$q_k(r_k) = q_{0,k}(r_k) - q_{i,k}(r_k)\,,\ \text{k=1, 2,} \tag{14}$$

here the indices 1 and 2 denote the surfaces of any adjacent ribbons facing each other.

In the case of radiative heat exchange between two parallel diffuse-gray surfaces the effective radiative flux $q_{0,k}(r_k)$ is the sum of self radiation and reflected radiation fluxes and fits a system of integral equations [2]:

$$q_{0,k}(r_k) = \varepsilon_k\sigma T_k^4(r_k) + (1-\varepsilon_k)q_{i,k}(r_k)\,, \tag{15}$$

$$q_{0,1}(y) - (1-\varepsilon)\frac{1}{2}\int_0^L q_{0,2}(x)\frac{b^2}{[(x-y)^2 + b^2]^{3/2}}dx = \sigma\left(\varepsilon T_1^4(y) + (1-\varepsilon)T_R{}^4\right), \tag{16}$$

$$q_{0,2}(y)-(1-\varepsilon)\frac{1}{2}\int_0^L q_{0,1}(x)\frac{b^2}{[(x-y)^2+b^2]^{3/2}}dx=\sigma\left(\varepsilon T_2^4(y)+(1-\varepsilon)T_R^4\right), \tag{17}$$

here $T_R^4=T_S^4\cdot\frac{1}{2}\left[1-\frac{y}{\sqrt{y^2+b^2}}\right]$, $b=d+2a-h_1^{(2)}-h_2^{(1)}$.

We determine the values $q_{0,1}$ and $q_{0,2}$ solving this system of equations. Then we determine the values of resultant radiative fluxes q_1 and q_2 :

$$q_k(y)=\frac{\varepsilon}{1-\varepsilon}(\sigma T_k^4(y)-q_{0,k}(y)), \tag{18}$$

If to use falling fluxes we determine $q_{i,k}$ as follows :

$$q_k(y)=\varepsilon(\sigma T_k^4(y)-q_{i,k}(y))=\varepsilon\sigma(T_k^4-T_{ck}^4), \tag{19}$$

here $T_{c\,k}=\sqrt[4]{q_{i,k}/\sigma}$, k=1, 2, (20) and we produce radiation law similar to (4) but only with other ambient temperatures T_{ck} .

So, heat exchange for the inner ribbons will be described by the expression (4) if consider $T_c=T_{ck}$. The impurity concentration in the melt is described by the equation:

$$\overset{\circ}{D}\Delta C-V\nabla C=0 \tag{21}$$

and the boundary conditions:

$$\frac{\partial C}{\partial y}=0,\ (x,y)\in\Gamma_1\cup\Gamma_3,\ C=C_0,\ (x,y)\in\Gamma_2,\ \frac{\partial C}{\partial\vec{n}}=0,\ (x,y)\in\Gamma_4\cup\Gamma_6,\ -\overset{\circ}{D}\frac{\partial C}{\partial\vec{n}}=V_0(k_0-1)C,\ (x,y)\in\Gamma_5.$$

A stress function F is introduced for the determination of the thermal stresses σ_x, σ_y, σ_{xy} by the formulae:

$$\sigma_x=\frac{\partial^2 F}{\partial y^2},\ \sigma_y=\frac{\partial^2 F}{\partial x^2},\ \sigma_{xy}=\frac{\partial^2 F}{\partial x\partial y} \tag{22}$$

In the case of a plain strain state F satisfies the relation:

$$\Delta^2 F=\frac{E}{1-\nu}\alpha_t\Delta T_2,\ (x,y)\in D_2, \tag{23}$$

The boundary conditions for F may be found requiring that there are no surface forces:

$$F=0,\ \frac{\partial F}{\partial\vec{n}}=0\ . \tag{24}$$

The solution of this problem by the finite element method is described in [3-5].

3 Numerical results

The numerical analysis has shown that the angle of inclination of the working edges of the dies influences significantly on the such characteristics of the pulling process as position and shape of the crystallization front, hydrodynamics of the melt and impurity distribution in the liquid menisci.

We have considered the package of six ribbons with distances between the dies 0.25 cm for the angles of inclination 5°, 20°, 30°, 45° and 60°. Fronts of crystallization calculated under these conditions are shown in

figure 2. This figure shows that with increasing of the angle of inclination the height of the front of crystallization decreases approximately from 0.18 mm to 0.12 mm at the first (external) ribbon and from 0.235 mm to 0.175 mm at the second and third ribbons. It should be noticed, larger angles of inclination result in larger difference from the planar shape of the fronts of crystallization.

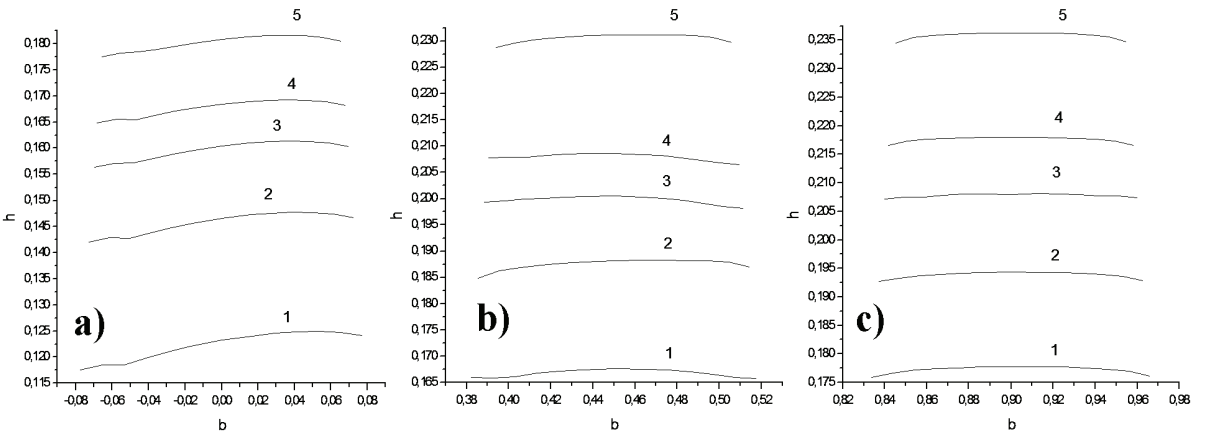

Fig. 2 Positions and shapes of the crystallization fronts (a – for the first crystal, b – for the second crystal, c – for the third crystal) with angles of inclination of the working edges of the dies : curve 1 - 60º, curve 2 - 45º, curve 3 - 30º, curve 4 - 20º, curve 5 - 5º. Axis X presents the current width *b (cm)* of the crystal, axis Y presents the height *h (mm)* of the crystallization fronts.

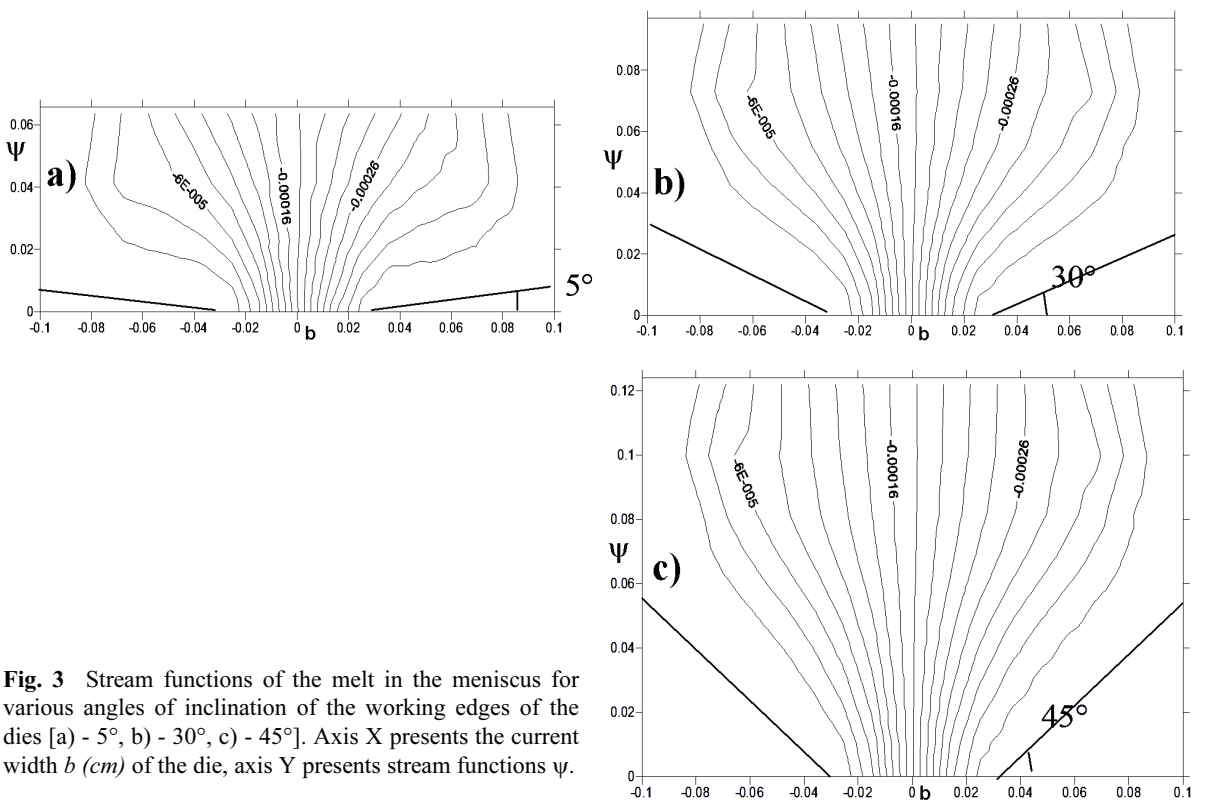

Fig. 3 Stream functions of the melt in the meniscus for various angles of inclination of the working edges of the dies [a) - 5°, b) - 30°, c) - 45°]. Axis X presents the current width *b (cm)* of the die, axis Y presents stream functions ψ.

Then the case has been considered when the distance between first and second dies was 1 cm, while the other distances were as before 0.25 cm. As a result, there was noticed decreasing the menisci heights in the all inner crystals approximately in 0.05 mm and 0.1 mm – in the external ribbons. There was no any significant changes in the shape of crystallization fronts.

The angle of inclination of the working edges of the dies influences significantly on the hydrodynamics of the melt in the liquid menisci. Really, increasing the angle of inclination results in the increasing the area of the melt stream. Melt streams at the dies outlet near the crystallization front may be not so significant if the angle of inclination is large enough (Fig. 3). This figure shows the melt streams are more uniform in the area far from the dies. That, of course, influences on the behavior of the impurity.

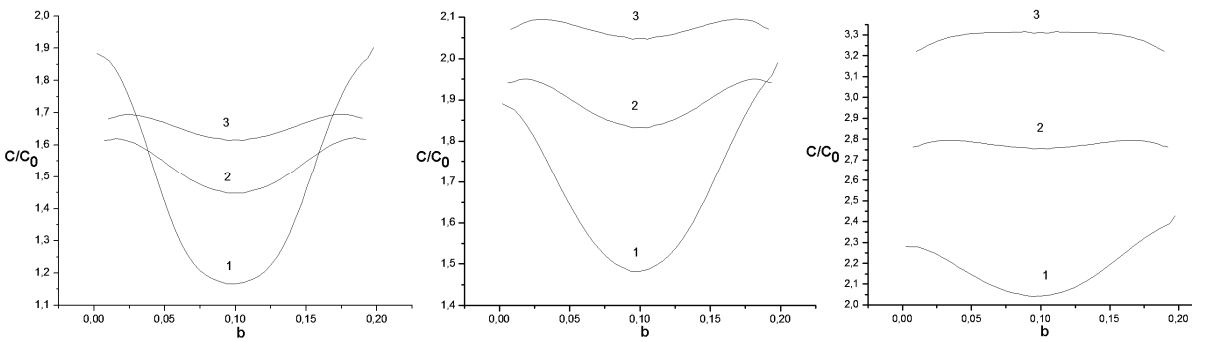

Fig. 4 Impurity concentration on the crystallization front (angles of inclination of the working edges of the dies : a – 5°, b –30°, c – 45°) : curve 1 – first crystal; curve 2 – second crystal; curve 3 – third crystal. Axis X presents the current width *b (cm)* of the crystal, axis Y presents impurity concentration C/C_0.

Behavior of the impurity at the crystallization front is the most important, because it defines the segregation of impurities in the crystal. Figure 4 shows the distribution of the impurity at the crystallization front. Impurities are distributed mostly non-uniformly in the first crystal. Second and third crystals have like behaviors of the impurities and the values of the concentrations of the impurities along the crystallization fronts increase significantly with the increase of the angle of inclination. The inner crystals may have larger values of the impurity concentrations in the center under the large angles of inclination than the external ribbons. Such behavior of the concentrations may be explained by the various heights of the liquid menisci and their hydrodynamics.

Thus, mathematical model of the distributions of the temperatures, impurity concentrations and thermal stresses in the course of the multi-run growth of sapphire ribbons by the EFG (Stepanov) technique in dependence on the various angles of inclination of the working edges of the dies is considered. Various values of the growth parameters have been analyzed for the purpose of optimization of the pulling process on the basics of the mathematical modeling. It has been determined that reduction of the distances between the dies results in the decreasing the difference in temperature distributions in the sapphire ribbons. This difference may be reduced by the use of the thermal screens substituting the external ribbons. The temperature of the working edges of the dies should not be decreased strongly to prevent large increase of the impurity concentrations. The temperature decrease may be observed indirectly by the measuring the menisci heights using the crystals weight sensor. Increasing the angle of inclination of the working edges of the dies results in the decreasing the menisci heights and, consequently, in the large stability of the crystal growth process.

Calculations of thermal stresses showed that they are concentrated near the crystallization front and lateral surface of the ribbon. The normal stress, σ_x, is a maximum near the center of the ribbon in the crystallization front and drops drastically towards the upper end of the crystal. The normal stress, σ_y, reaches its maximum on the lateral surface near the crystallization front and decreases gradually with crystal length. The tangential stress, σ_{xy}, is a maximum at some distance from the front and its magnitude is approximately in order less than that of the normal stresses. In general, the stress magnitude and exact location of its maximum points are found to depend on ambient temperature, the length of crystals, the position of a certain ribbon, the temperature of the die top face, the gap between adjacent sub-dies, the angle of inclination of the working surface of the sub-dies.

Calculations showed, thermal stresses in ribbons vary significantly over the crystal package and weakly with variation of the angle of inclination of the working surface of the die, namely, they increase slightly with increase of the angle of inclination. This increase is approximately 0.1 Mpa for the stresses σ_x and σ_y in the

range of the angle change from 0° to 45°. Relating to the variation of the stresses over the package consisting in 6 ribbons, the thermal stresses in outer ribbons are significantly larger than in inner ribbons under our considered temperature regime and die geometry, and can be larger in two-three times than in inner ribbons. It should be noticed, thermal stresses in the inner ribbon practically have no difference. Thus the first ribbon is being as a thermal screen for the inner ribbons.

4 Nomenclature

a	half-thickness of die
A	constant being determined from the condition of equality of the melt streams through the capillary channel and crystallization front
b	half-thickness of the crystal ribbons
c	heat capacity
C	impurity concentration
d	distance between neighboring dies
d_0	half-width of capillary channel
D	calculation area
$\overset{o}{D}$	diffusion coefficient
D^t	deformation tensor
f	meniscus profile curve
F	external specific force
g	gravity acceleration
H	crystallization front curve
H_{ef}	distance between melt surface and meniscus base line
$h_2^{(1)}$ and $h_1^{(2)}$	magnitudes calculating from **y-**axis up to lateral neighboring surfaces of the ribbons
k_i	thermal conductivity
k_0	impurity segregation coefficient
l	current length of the crystals
L	length of the ribbons in the package
N	number of the ribbons in the package
$\vec{n}$	normal vector to the boundary of the calculation area
P	external pressure in the melt
q	radiative stream
T	temperature
T_R	temperature being influenced by T_s
T_S	known temperature of the surface of the common base between two neighboring dies
u_1	normal (to the boundary) component of the melt rate
v	tangential (to the boundary) component of the melt rate
V_0	pulling rate of the crystals
α_t	thermal expansion coefficient
β	angle of the inclination of the working edges of the dies
Γ	boundary of the calculation area
ΔH_f	specific latent heat of fusion
ε_i	emissivity coefficient
ε_0	growth angle
ζ	heat exchange coefficient
η_i	heat transfer coefficient
μ	dynamic viscosity of the melt

ν	Poisson's coefficient
ρ_i	density
σ	Stefan-Boltzmann constant
$\sigma_{liq,g}$	surface tension coefficient of the melt
$\vec{\tau}$	tangential vector to profile curve of the meniscus
ψ	melt stream function

References

[1] A. V. Borodin, A. V. Zhdanov, L. P. Nikolaeva, I. S. Petkov, and L. P. Chupiatova, Inzhenerno-Fizichesky Zhurnal **74**, 106 (2001).
[2] G. Strang and G. J. Fix, An Analysis of the Finite Element Method, Prentice-Hall, Englewood Cliffs, 1973.
[3] R. Zigel and J. Howell, Thermal Heat Transfer by Radiation (Moscow, 1975).
[4] C. A. J. Eletcher, Computational Galerkin Methods. New York, Berlin, Heidelberg, Tokio: Springer, 1984.
[5] A. R. Mitchell and R. Wait, The Finite-Element Method in Partial Differential Equations (Wiley, Chichester, New York, Brisbane, Toronto, 1977).

